Electrocatalysis

DOI: 10.1002/anie.201407131

Single-Site Copper(II) Water Oxidation Electrocatalysis: Rate Enhancements with HPO_4^{2-} as a Proton Acceptor at pH 8**

*Michael K. Coggins, Ming-Tian Zhang, Zuofeng Chen, Na Song, and Thomas J. Meyer**

Abstract: *The complex $Cu^{II}(Py_3P)$ (**1**) is an electrocatalyst for water oxidation to dioxygen in $H_2PO_4^-/HPO_4^{2-}$ buffered aqueous solutions. Controlled potential electrolysis experiments with **1** at pH 8.0 at an applied potential of 1.40 V versus the normal hydrogen electrode resulted in the formation of dioxygen (84 % Faradaic yield) through multiple catalyst turnovers with minimal catalyst deactivation. The results of an electrochemical kinetics study point to a single-site mechanism for water oxidation catalysis with involvement of phosphate buffer anions either through atom–proton transfer in a rate-limiting O—O bond-forming step with HPO_4^{2-} as the acceptor base or by concerted electron–proton transfer with electron transfer to the electrode and proton transfer to the HPO_4^{2-} base.*

The oxidation of water to dioxygen is a key half-reaction in natural photosynthesis and a considerable challenge for artificial photosynthetic schemes aimed at converting solar energy into fuels for energy conversion and storage. Microscopically, water oxidation is necessarily complex since it involves the loss of four electrons and four protons with formation of an O—O bond ($2H_2O \rightarrow O_2 + 4H^+ + 4e^-$, $E^0 = 1.23$ V vs. NHE, $E_{pH\,7} = 0.82$ V vs. normal hydrogen electrode, NHE).

Considerable progress has been made in catalyzing this reaction by using transition-metal complexes. Examples of Ru,[1] Ir,[2] Fe,[3] Co,[4] and Mn[5] complexes have been identified as single-site or multi-site catalysts in solution or immobilized on metal-oxide surfaces, or as precursors to catalytically active metal oxides or films. Practical strategies for light-driven water oxidation in solar fuel applications require robust and selective catalysts that react at appreciable rates at low overpotentials and do not compete for light absorption with an integrated chromophore or chromophore antenna. Molecular catalysts are particularly attractive in these applications since their catalytic properties can be relatively fine-tuned by systematic structural and electronic modifications, and strategies are available for incorporating them into chromophore–catalyst assemblies.

A few recent reports have documented the first examples of Cu^{II}-mediated water oxidation electrocatalysis with simple Cu^{II} complexes or salts.[6] Cu^{II} water oxidation catalysis is appealing since Cu is biologically relevant and abundant with a well-defined coordination chemistry.

Here we report that the monomeric Cu^{II} complex $Cu^{II}(Py_3P)$ (**1**, Py_3P is *N*,*N*-bis(2-(2-pyridyl)ethyl)pyridine-2,6-dicarboxamidate, Figure 1) is a stable water oxidation electrocatalyst in $H_2PO_4^-/HPO_4^{2-}$ buffered solutions. A combination of cyclic voltammetry and controlled-potential electrolysis (CPE) measurements provide experimental evidence for a single-site water oxidation mechanism involving either rate-determining atom–proton transfer or concerted electron–proton transfer leading to rapid water oxidation through multiple catalytic turnovers.

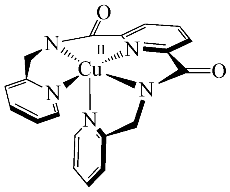

Figure 1. Structure of $Cu^{II}(Py_3P)$ (**1**).

The electrochemical properties of **1** were explored by CV measurements at a boron-doped diamond (BDD) working electrode in water at a constant ionic strength ($\mu = 0.5$ M) with added $LiClO_4$. As shown in Figure 2, cyclic voltammograms (CVs) of **1** at pH 8.0 in a 0.1 M $H_2PO_4^-/HPO_4^{2-}$ buffer solution includes two irreversible anodic waves with $E_{p,a,1} = 1.29$ V versus NHE and $E_{p,a,2} = 1.50$ V versus NHE that show little variation in potential with changes in CV scan rates between 10–100 $mV\,s^{-1}$. The current densities (j) for both are greatly enhanced relative to the BDD electrode background (see Figure S1 in the Supporting Information). The first oxidative wave, $E_{p,a,1}$, remains irreversible even if the switching potential is reduced to 1.4 V. CV measurements show that $E_{p,a,1}$ decreases by 56 mV per pH unit from pH 3–7, which is close to the decrease of 59 mV per pH unit predicted by the Nernst equation for a $1e^-/1H^+$ redox couple. $E_{p,a,1}$ is pH-independent from pH 7–12 (Figures S2,3). The Pourbaix diagram ($E_{p,a}$ vs. pH) for this couple, Figure S3, is consistent with $pK_a = 7$ for $Cu^{II}(OH_2)$, coincidentally close to pK_a about

---

[*] Dr. M. K. Coggins, Prof. M.-T. Zhang,[+] Prof. Z. Chen,[++] Dr. N. Song, Prof. T. J. Meyer
Department of Chemistry
University of North Carolina at Chapel Hill
Chapel Hill, NC 27516 (USA)
E-mail: tjmeyer@unc.edu

[+] Current address: Center of Basic Molecular Science (CBMS)
Department of Chemistry, Tsinghua University
Beijing (China)

[++] Current address: Department of Chemistry, Tongji University
Shanghai, 200092 (China)

[**] Funding by the Center for Catalytic Hydrocarbon Functionalization, an Energy Frontier Research Center (EFRC), funded by the U.S. Department of Energy (DOE), Office of Science, Office of Basic Energy Sciences, under award number DE-SC0001298 is gratefully acknowledged for supporting M.K.C. Funding by the UNC EFRC Center for Solar Fuels, an EFRC funded by the U.S. DOE, Office of Science, Office of Basic Energy Sciences, under award number DE-SC0001011 is gratefully acknowledged for supporting M.-T.Z., Z.C., and N.S.

Supporting information for this article is available on the WWW under http://dx.doi.org/10.1002/anie.201407131.

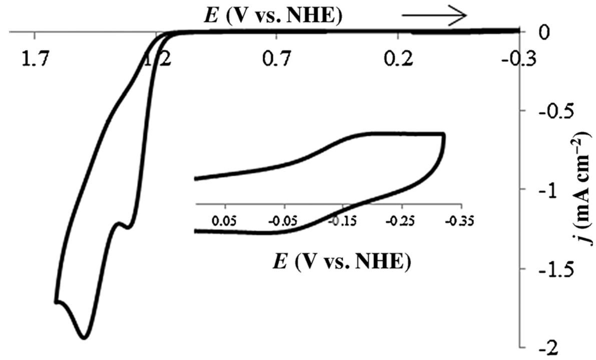

Figure 2. Cyclic voltammogram of $Cu^{II}(Py_3P)$ (**1**, 0.7 mM) at pH 8.0 (0.1 M phosphate buffer, $\mu = 0.5$ M) at a boron-doped diamond working electrode (BDD, 0.07 cm^2, 100 mV s^{-1}, 293 K) with the arrow indicating the initial scan direction. The inset shows a magnified view of the $Cu^{II/I}$ wave at −0.14 V versus NHE.

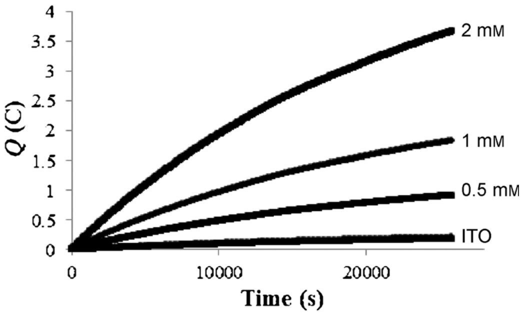

Figure 3. Chronocoulometric (Q = charge vs. time) plot from controlled-potential electrolysis with $Cu^{II}(Py_3P)$ ([**1**] = 2 mM, 1 mM, and 0.5 mM) at a tin-doped indium oxide working electrode (ITO, 0.7 cm^2) and pH 8.0 (0.1 M phosphate, $\mu = 0.5$ M with added $LiClO_4$) at an applied potential of 1.4 V versus NHE. A charge-versus-time trace for the background ITO electrode is also shown.

7 for $Cu^{II}(H_2O)_6{}^{2+}$.[7] $E_{p,a,2}$ is pH-independent from pH 3–12 (Figures S2,3).

CVs of **1** at pH 8.0 (deoxygenated 0.1 M phosphate buffer, $\mu = 0.5$ M with added $LiClO_4$) under nitrogen include a quasi-reversible, pH-independent $Cu^{II/I}$ couple at $E_{1/2} = -0.14$ V versus NHE ($\Delta E = 120$ mV, Figure 2, Figure S3). A diffusion coefficient (D_{Cu}) of 6×10^{-5} cm^2 s^{-1} was determined for **1** from the dependence of the anodic peak current ($i_{p,a}$) for the $Cu^{II/I}$ couple on scan rate ($\nu^{1/2}$) by application of the Randles–Sevcik relation[8] in Equation (1) (Figure S4). In Equation (1), n (= 1e$^-$) is the number of electrons transferred, F is the Faraday constant, A is the area of the working electrode (0.07 cm^2), R is the ideal gas constant, and T is the temperature.

$$i_p = 0.4463\, n\, F A [\mathbf{1}] [(n F \nu D_{Cu})/(R T)]^{1/2} \quad (1)$$

To determine if **1** was capable of catalytic water oxidation to dioxygen, CPE experiments were conducted in a closed, deoxygenated three-compartment electrolysis cell at a tin-doped indium oxide (ITO, 0.7 cm^2) working electrode at pH 8.0 with a 0.1 M phosphate buffer, $[H_2PO_4^-]/[HPO_4^{2-}] = 3.8\times10^{-2}$, and $\mu = 0.5$ M with added $LiClO_4$ and various concentrations of **1**. Sustained current densities between 0.2–0.3 mA cm^{-2} were maintained over a minimum of 7 h with $[\mathbf{1}]_0 = 2$ mM at an applied potential of 1.4 V versus NHE (640 mV overpotential). After 7 h of electrolysis, the reaction headspace was sampled and analyzed by gas chromatography/mass spectrometry to reveal that 7 μmoles of O_2 had been produced in 84 % Faradaic yield (19 turnovers) assuming a 4e$^-$ catalytic process and after correcting for background O_2 from cell leakage with no detectable amounts of CO or CO_2 (Figure S5). Note that the calculated Faradaic yield should be considered a lower limit, as some of the O_2 produced during electrolysis is solubilized in the electrolyte and not detected by headspace sampling.

Additional CPE experiments under these conditions showed that the total charge passed after 7 h of electrolysis varied linearly with the initial catalyst concentration, $[\mathbf{1}]_0$, with no evidence for an induction period at early electrolysis times, providing additional evidence for homogeneous single-site water oxidation catalysis (Figure 3). The absence of an induction period is also consistent with the similarities between steady-state current densities measured by chronoamperometry at various potentials and those measured from slow scan-rate CVs (10 mV s^{-1}), further pointing to catalyst stability (Figure S6). Charges passed during the CPE experiments were due predominantly to **1** and not free Cu^{II}, which has been shown to be a water oxidation catalyst with high concentrations of added carbonate.[6d] Under the experimental conditions used herein, Cu^{II} immediately precipitates as $Cu_3(PO_4)_2$ ($K_{sp} = 1.40\times10^{-37}$) and displays no catalytic activity toward water oxidation (see Figure S7).[6b–d]

Only a 10 % loss of the catalyst occurred during the CPE experiments as shown by UV/Vis absorption spectral comparisons before and after each electrolysis experiment (Figure 3, Figure S8). A pseudo-first-order rate constant for catalyst decomposition of 3×10^{-6} s^{-1} was determined from a plot of ln[**1**] versus time by monitoring UV/Vis spectral changes during electrolysis (Figure S9). CVs of the electrolyte mixture before and after 7 h of electrolysis at a BDD working electrode showed a 10 % decrease in current density for the anodic waves without signs of new waves in the CV scans from an additional electroactive form (Figure S10). CVs of the ITO working electrode before and after each electrolysis experiment in the absence of catalyst were essentially identical with no evidence for electroactive or insulating films adsorbed to the electrode surface during the electrolysis (Figure S11). The lack of evidence for a new electroactive species which is either adsorbed on the working electrode or present in the electrolyte mixture is collectively consistent with homogeneous catalysis.

Cyclic voltammetry measurements revealed that anodic current densities at 1.50 and 1.29 V versus NHE, respectively, vary linearly with [**1**] at pH 8.0 (0.1 M phosphate buffer, $[HPO_4^{2-}] = 0.09$ M, $\mu = 0.5$ M with added $LiClO_4$, Figure 4). A first-order dependence is consistent with a single-site mechanism for water oxidation catalysis and the dependence of the catalytic current (i_{cat}) on the catalyst concentration shown in Equation (2).[8] In Equation (2), n_{cat} is the number of electrons

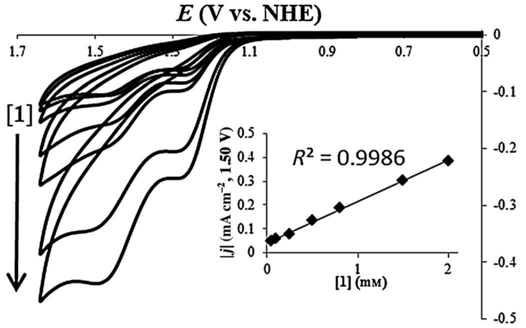

Figure 4. Cyclic voltammograms of $Cu^{II}(Py_3P)$ (**1**) as a function of increasing catalyst concentration (arrow) at pH 8.0 (0.1 M phosphate buffer, $[HPO_4^{2-}] = 0.09$ M, $\mu = 0.5$ M with added $LiClO_4$) at a boron-doped diamond working electrode (BDD, 0.07 cm^2, 30 $mV\,s^{-1}$, 293 K). The inset shows a plot of current density magnitude ($|j|$) versus [**1**] at 1.50 V versus NHE.

$$i_{cat} = n_{cat} F\,A[\mathbf{1}](k_{cat} D_{Cu})^{1/2} \qquad (2)$$

transferred ($n = 4e^-$). From cyclic voltammetry measurements over a catalyst concentration range of 0.05–2 mM, there was no evidence for additional redox active Cu species, the ratio of peak currents at $E_{p,a,1}$ and $E_{p,a,2}$ remained constant, and catalysis was dominated by first-order kinetics. A comparison of scan-rate-normalized CVs ($i/\nu^{1/2}$) shows a decrease in i with increased ν at high potentials, which is consistent with a contribution to the current from a rate-limiting chemical step or steps preceding diffusional electron transfer (Figure S12).[8]

The current density at 1.50 V versus NHE at constant [**1**] was found to vary linearly with $[HPO_4^{2-}]$ at pH 8.0 at a fixed ratio of $[H_2PO_4^-]/[HPO_4^{2-}]$ (Figure S13). The dependence on $[HPO_4^{2-}]$ provides kinetic evidence for a pathway that is first order in $[HPO_4^{2-}]$ as found earlier for Ru^{II}–polypyridyl catalysts.[9] There were no signs of catalyst anation with $[HPO_4^{2-}]$ up to 0.2 M. The current density was invariant to changes in pH between pH 7–8.2 ($[OH^-] = 6\times10^{-9}$–10^{-7} M) at fixed $[HPO_4^{2-}]$ and fixed [**1**] (Figure S14).

The appearance of general base catalysis in water oxidation is well established for single-site Ru^{II} and Co^{II} complexes.[4a,9] For Ru^{II}–polypyridyl complexes, this dependence has been attributed to atom–proton transfer (APT) with O–O bond formation occurring in concert with proton transfer to the hydrogen-bonded base (Scheme 1).

Collectively, the data on $Cu^{II}(Py_3P)$ water oxidation catalysis are consistent with the rate and rate constant expressions in Equations (3) and (4), respectively. In Equations (3) and (4), k_{cat} is the catalytic rate constant for water oxidation, k_B is the buffer base-dependent rate constant, and

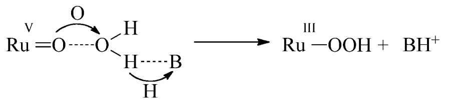

Scheme 1. Atom–proton transfer in catalytic water oxidation by single-site ruthenium(V)-oxo complexes.[9]

k_{H_2O} is the rate constant in the absence of an added buffer base. Catalytic rate constants were evaluated from variable scan rate cyclic voltammetry measurements conducted with 0.5–1 mM **1** at pH 8.0 with varying concentrations of HPO_4^{2-}. Tafel plots were constructed from CV data at the onset of catalytic current (foot-of-the-wave) and extrapolated to obtain i_{cat} values at 1.50 V versus NHE (760 mV overpotential, Figure S15).[10] Tafel plots constructed from cyclic voltammetry data measured between 1.23 and 1.33 V gave comparable i_{cat} values when extrapolated to 1.50 V. Measured currents were normalized with cathodic i_p values for the $Cu^{II/I}$ couple (−0.07 V vs. NHE) and fit to the expression in Equation (5); see Figure S14. Plots of i_{cat}/i_p versus $\nu^{-1/2}$ were

$$i_{cat}/i_p = 2.242\,n_{cat}(k_{cat}R\,T/n\,F\nu)^{1/2} \qquad (5)$$

used to evaluate k_{cat}. As shown in Figure 5, k_{cat} varies linearly with $[HPO_4^{2-}]$ up to at least 0.2 M HPO_4^{2-} with $k_B = 1.9\times10^2\,M^{-1}\,s^{-1}$ and $k_{H_2O} = 3.2\times10^{-1}\,s^{-1}$; note Equation (4). The

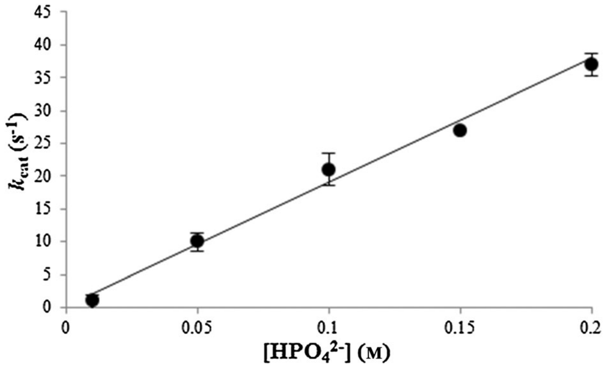

Figure 5. Plot of the catalytic rate constant (k_{cat}) versus $[HPO_4^{2-}]$ (M) for water oxidation by $Cu^{II}(Py_3P)$ (**1**) at pH 8.0 ($\mu = 0.5$ M with added $LiClO_4$) at room temperature.

three orders of magnitude difference between k_B with $B = HPO_4^{2-}$ and k_{H_2O} is consistent with an APT pathway given the difference in the proton-accepting ability of HPO_4^{2-} with $pK_a(H_2PO_4^-) = 7.2$ compared to H_2O with $pK_a(H_3O^+) = -1.74$. Similar observations have been made for the APT O–O bond-forming step in water oxidation by $[Ru(Mebimpy)(bpy)(H_2O)]^{2+}$ (Mebimpy is 2,6-bis(1-methylbenzimidazol-2-yl)pyridine and bpy is 2,2′-bipyridine)[9b] and $[Ru(tpy)(bpz)(OH)]^+$ (tpy = 2,2′:6,2″-terpyridine and bpz = 2,2′-bipyrazine).[11] A kinetic isotope effect (KIE, $k_{cat,H_2O}/k_{cat,D_2O}$) of 2 was determined by using Equation (6) and current comparisons at 1.50 V at pH 8.0 relative to pD 8.0 in 0.1 M phosphate-buffered solutions ($\mu = 0.5$ M with added $LiClO_4$ at 293 K). The magnitude of the KIE is consistent with proton involvement in the rate-limiting step and a possible APT pathway for water oxidation by **1** (Figure S16).

$$\text{rate} = k_{cat}[\mathbf{1}] \qquad (3)$$

$$k_{cat} = k_B[HPO_4^{2-}] + k_{H_2O} \qquad (4)$$

$$\mathrm{KIE} = k_{\mathrm{cat,H_2O}}/k_{\mathrm{cat,D_2O}} = (i_{\mathrm{cat,H_2O}}/i_{\mathrm{cat,D_2O}})^2 \tag{6}$$

The experimental data are consistent with two electron oxidative activation of **1**, which triggers electrocatalytic water oxidation. At pH 8.0, **1** exists as d^9 $\mathrm{Cu^{II}(OH)^-}$ with oxidation to d^8 $\mathrm{Cu^{III}(OH)}$ occurring at 1.29 V versus NHE ($E_{\mathrm{p,a,1}}$). The electron-transfer irreversibility of this oxidation may be due in, because of significant catalyst structural change, as a d^8 $\mathrm{Cu^{III}}$ complex. Once formed, $\mathrm{Cu^{III}(OH)}$ undergoes further oxidation at 1.50 V versus NHE ($E_{\mathrm{p,a,2}}$) to give a second intermediate. There is no literature precedence for a catalytically active single-site $\mathrm{Cu^{III}}$ complex for water oxidation, and a plausible interpretation of the catalytic CV waveform is that $E_{\mathrm{p,a,1}}$ gains current intensity by lying on top of a catalytic wave for water oxidation catalysis from a twice-oxidized intermediate with $E_{\mathrm{p,a,1}} = 1.29$ V. The possibility that the first oxidative process ($E_{\mathrm{p,a,1}}$) does result in at least a contribution to water oxidation, however, cannot be definitively excluded based upon the cyclic voltammetry data.

The electronic formulation of the twice-oxidized intermediate is unclear. Oxidation of $\mathrm{Cu^{III}(OH)}$ could give either d^7 $\mathrm{Cu^{IV}(OH)^+}$ or ligand-oxidized d^8 $\mathrm{Cu^{III}(Py_3P^{\bullet+})(OH)^+}$ [Eq. (7)]. An alternate explanation based upon the first-order buffer base pathway is rate-limiting concerted electron–proton transfer (EPT). Electron transfer to the electrode with proton transfer to $\mathrm{HPO_4^{2-}}$ would give a d^8 $\mathrm{Cu^{III}(O^{\bullet+})}$ or d^7 $\mathrm{Cu^{IV}(O)}$ intermediate [Eqs. (8),(9)].[9a,12]

$$\mathrm{Cu^{III}(Py_3P)(OH)} \xrightarrow{-e^-} \mathrm{Cu^{IV}(Py_3P)(OH)^+} \text{ or } \mathrm{Cu^{III}(Py_3P^{\bullet+})(OH)^+} \tag{7}$$

$$\mathrm{Cu^{III}(Py_3P)(OH) + HPO_4^{2-} \rightarrow Cu^{III}(Py_3P)(OH)\cdots OP(O)_2OH^{2-}} \tag{8}$$

$$\mathrm{Cu^{III}(Py_3P)(OH)\cdots OP(O)_2OH^{2-}} \xrightarrow{-e^-} \mathrm{H_2PO_4^- + Cu^{III}(Py_3P)(O^{\bullet+})} \text{ or } \mathrm{Cu^{IV}(Py_3P)(O)} \tag{9}$$

There is no direct experimental evidence for $\mathrm{Cu^{IV}(OH)}$ or $\mathrm{Cu^{IV}(O)}$ as kinetic intermediates. The latter has been proposed as a possible intermediate in Cu-mediated electrocatalytic water oxidation.[6c] A non-innocent ligand redox effect has been proposed in water oxidation electrocatalysis by (6,6′-(HO)$_2$bpy)Cu(OH)$_2$ (6,6′-(HO)$_2$bpy is 6,6′-dihydroxy-2,2′-bipyridine) with a $\mathrm{Cu^{III}(OH)}$-bpy radical cation proposed as the catalytically-active intermediate.[6a]

With either $\mathrm{Cu^{IV}(OH)^+}$ or $\mathrm{Cu^{III}(Py_3P^{\bullet+})(OH)^+}$ as the twice-oxidized intermediate, subsequent rate-limiting APT O−O bond formation with proton transfer to $\mathrm{HPO_4^{2-}}$ would give a d^9 $\mathrm{Cu^{II}(H_2O_2)}$ intermediate [Eqs. (10),(11)]. Water attack on either $\mathrm{Cu^{III}(O^{\bullet+})}$ or $\mathrm{Cu^{IV}(O)}$ would give the same $\mathrm{Cu^{II}(H_2O_2)}$ intermediate [Eq. (12),(13)]. In the water oxidation cycle, further oxidation of the proposed $\mathrm{Cu^{II}(H_2O_2)}$ intermediate would lead to $\mathrm{O_2}$ release, $\mathrm{H_2O}$ coordination, and re-entry of $\mathrm{Cu^{II}(Py_3P)(OH)}$ into the catalytic cycle [Eq. (14)].

$$\mathrm{Cu^{IV}(Py_3P)(OH) + H\text{-}O\text{-}H\cdots OP(O)_2OH \rightarrow Cu^{II}(Py_3P)(H_2O_2) + H_2PO_4^-} \tag{10}$$

$$\mathrm{Cu^{III}(Py_3P^{\bullet+})(OH) + H\text{-}O\text{-}H\cdots OP(O)_2OH \rightarrow Cu^{II}(Py_3P)(H_2O_2) + H_2PO_4^-} \tag{11}$$

$$\mathrm{Cu^{III}(Py_3P)(O^{\bullet+}) + H_2O \rightarrow Cu^{II}(Py_3P)(H_2O_2)} \tag{12}$$

$$\mathrm{Cu^{IV}(Py_3P)(O) + H_2O \rightarrow Cu^{II}(Py_3P)(H_2O_2)} \tag{13}$$

$$\mathrm{Cu^{II}(Py_3P)(H_2O_2) + 2\,HPO_4^{2-} + H_2O} \xrightarrow{-2e^-} \mathrm{Cu^{II}(Py_3P)(H_2O) + O_2 + 2\,H_2PO_4^-} \tag{14}$$

There is no direct experimental evidence for a Cu-peroxide intermediate, but such intermediates are well documented as products of reactions between $\mathrm{Cu^{I}}$ complexes and $\mathrm{O_2}$.[13] Evidence for a peroxide intermediate has been found in water oxidation electrocatalysis by $\mathrm{(TGG)Cu^{II}(OH_2)^{2-}}$ (TGG is triglycylglycine).[6c]

Our results demonstrate that $\mathrm{Cu^{II}(Py_3P)}$ is an effective electrocatalyst for water oxidation to dioxygen. It continues to react through multiple turnovers with high Faradaic efficiencies in near neutral phosphate buffered solutions. The rate constant ratio of catalyzed water oxidation to deactivation ($k_{\mathrm{cat.}}/k_{\mathrm{deact.}}$ about $6\times10^7\ \mathrm{s^{-1}}$) is impressive, pointing to stable long term performance. Also impressive is the rate of electrocatalytic water oxidation under these conditions with a calculated half time ($t_{1/2}$) of 1.8×10^{-2} s ($k_{\mathrm{cat}} = 38\ \mathrm{s^{-1}}$) for water oxidation with 0.2 M $\mathrm{HPO_4^{2-}}$. Its reactivity under these conditions compares well with the few other Cu water oxidation catalysts in the literature, where k_{obs} values in the range of 10^1–$10^2\ \mathrm{s^{-1}}$ have been reported[6a,c,d] but at elevated pH (11–14) with high concentrations of added buffer bases and hydroxide. The direct involvement of hydroxide in O−O bond formation has been described for Ru–polypyridyl oxidants.[9]

The kinetic characteristics of water oxidation by **1** are consistent with a single-site mechanism with oxidative activation of the catalysts observed directly by CV measurements. It is notable that electrocatalytic water oxidation by **1** occurs at relatively low pH with added $\mathrm{HPO_4^{2-}}$, conditions that will allow a derivative to be incorporated into molecular assemblies for photoelectrochemical water oxidation.

Received: July 11, 2014

Keywords: copper · electrocatalysis · electrochemistry · homogeneous catalysis · water oxidation

---

[1] a) A. K. Vannucci, L. Alibabaei, M. D. Losego, J. J. Concepcion, B. Kalanyan, G. N. Parsons, T. J. Meyer, *Proc. Natl. Acad. Sci. USA* **2013**, *110*, 20918; b) M. R. Norris, J. J. Concepcion, Z. Fang, J. L. Templeton, T. J. Meyer, *Angew. Chem. Int. Ed.* **2013**, *52*, 13580; *Angew. Chem.* **2013**, *125*, 13825; c) L. L. Duan, F. Bozoglian, S. Mandal, B. Stewart, T. Privalov, A. Llobet, L. C. Sun, *Nat. Chem.* **2012**, *4*, 418; d) J. J. Concepcion, J. W. Jurss, M. K. Brennaman, P. G. Hoertz, A. O. T. Patrocinio, N. Y. M. Iha, J. L. Templeton, T. J. Meyer, *Acc. Chem. Res.* **2009**, *42*, 1954.
[2] a) U. Hintermair, S. W. Sheehan, A. R. Parent, D. H. Ess, D. T. Richens, P. H. Vaccaro, G. W. Brudvig, R. H. Crabtree, *J. Am. Chem. Soc.* **2013**, *135*, 10837; b) N. D. Schley, J. D. Blakemore, N. K. Subbaiyan, C. D. Incarvito, F. D'Souza, R. H. Crabtree,

G. W. Brudvig, *J. Am. Chem. Soc.* **2011**, *133*, 10473; c) J. F. Hull, D. Balcells, J. D. Blakemore, C. D. Incarvito, O. Eisenstein, G. W. Brudvig, R. H. Crabtree, *J. Am. Chem. Soc.* **2009**, *131*, 8730; d) W. Ruettinger, M. Yagi, K. Wolf, S. Bernasek, G. C. Dismukes, *J. Am. Chem. Soc.* **2000**, *122*, 10353.

[3] a) W. C. Ellis, N. D. McDaniel, S. Bernhard, T. J. Collins, *J. Am. Chem. Soc.* **2010**, *132*, 10990; b) J. L. Fillol, Z. Codola, I. Garcia-Bosch, L. Gomez, J. J. Pla, M. Costas, *Nat. Chem.* **2011**, *3*, 807; c) I. Garcia-Bosch, Z. Codolà, I. Prat, X. Ribas, J. Lloret-Fillol, M. Costas, *Chem. Eur. J.* **2012**, *18*, 13269; d) M. Z. Ertem, L. Gagliardi, C. J. Cramer, *Chem. Sci.* **2012**, *3*, 1293; e) R. Sarma, A. M. Angeles-Boza, D. W. Brinkley, J. P. Roth, *J. Am. Chem. Soc.* **2012**, *134*, 15371; f) M. K. Coggins, M.-T. Zhang, A. K. Vannucci, C. J. Dares, T. J. Meyer, *J. Am. Chem. Soc.* **2014**, *136*, 5531.

[4] a) D. Wang, J. T. Groves, *Proc. Natl. Acad. Sci. USA* **2013**, *110*, 15579; b) D. G. Nocera, *Acc. Chem. Res.* **2012**, *45*, 767; c) D. J. Wasylenko, C. Ganesmoorthy, J. Borau-Garcia, C. P. Berlinguette, *Chem. Commun.* **2011**, *47*, 4249.

[5] a) K. J. Young, M. K. Takase, G. W. Brudvig, *Inorg. Chem.* **2013**, *52*, 7615; b) G. C. Dismukes, R. Brimblecombe, G. A. N. Felton, R. S. Prydun, J. E. Sheats, L. Spiccia, G. F. Swiegers, *Acc. Chem. Res.* **2009**, *42*, 1935; c) Y. Gao, T. Akermark, J. Liu, L. Sun, B. Akermark, *J. Am. Chem. Soc.* **2009**, *131*, 8726.

[6] a) T. Zhang, C. Wang, S. Liu, J.-L. Wang, W. Lin, *J. Am. Chem. Soc.* **2014**, *136*, 273; b) Z. Chen, P. Kang, M.-T. Zhang, B. R. Stoner, T. J. Meyer, *Energy Environ. Sci.* **2013**, *6*, 813; c) M.-T. Zhang, Z. Chen, P. Kang, T. J. Meyer, *J. Am. Chem. Soc.* **2013**, *135*, 2048; d) Z. Chen, T. J. Meyer, *Angew. Chem. Int. Ed.* **2013**, *52*, 700; *Angew. Chem.* **2013**, *125*, 728; e) S. M. Barnett, K. I. Goldberg, J. M. Mayer, *Nat. Chem.* **2012**, *4*, 498; f) S. G. Winikoff, C. J. Cramer, *Catal. Sci. Technol.* **2014**, *4*, 2484.

[7] *Fate and Transport of Heavy Metals in the Vadose Zone* (Eds.: H. M. Selim, I. K. Iskandar), CRC, Boca Raton, FL, **1999**.

[8] *Electrochemical Methods: Fundamentals and Applications*, 2ednd ed(Eds.: A. J. Bard, L. R. Faulkner), Wiley, Hoboken, NJ, **2001**.

[9] a) N. Song, J. J. Concepcion, R. A. Binstead, J. A. Rudd, A. K. Vannucci, C. Dares, T. J. Meyer, *Inorg. Chem.*, submitted; b) Z. Chen, J. J. Concepcion, X. Hu, W. Yang, P. G. Hoertz, T. J. Meyer, *Proc. Natl. Acad. Sci. USA* **2010**, *107*, 7225.

[10] C. Costentin, S. Drouet, M. Robert, J.-M. Savéant, *J. Am. Chem. Soc.* **2012**, *134*, 11235.

[11] Y. Tamaki, A. K. Vannucci, C. J. Dares, R. A. Binstead, T. J. Meyer, *J. Am. Chem. Soc.* **2014**, *136*, 6854.

[12] a) D. R. Weinberg, C. J. Gagliardi, J. F. Hull, C. F. Murphy, C. A. Kent, B. C. Westlake, A. Paul, D. H. Ess, D. G. McCafferty, T. J. Meyer, *Chem. Rev.* **2012**, *112*, 4016; b) M. H. V. Huynh, T. J. Meyer, *Chem. Rev.* **2007**, *107*, 5004.

[13] a) E. A. Lewis, W. B. Tolman, *Chem. Rev.* **2004**, *104*, 1047; b) L. M. Mirica, X. Ottenwaelder, T. D. P. Stack, *Chem. Rev.* **2004**, *104*, 1013.